

# Memory Effects in Nonequilibrium Transport for Deterministic Hamiltonian Systems

**Jean-Pierre Eckmann<sup>1,2</sup>, Carlos Mejía-Monasterio<sup>1</sup> and Emmanuel Zabey<sup>1</sup>**

<sup>1</sup>Département de Physique Théorique, Université de Genève

<sup>2</sup>Section de Mathématiques, Université de Genève

## Abstract

We consider nonequilibrium transport in a simple chain of identical mechanical boxes in which particles move around. In each box, there is a rotating disc, with which these particles interact, and this is the only interaction in the model. It was shown in [1] that to a good approximation, the jump rates of particles and the energy-exchange rates from cell to cell follow linear profiles. Here, we refine that study, by analyzing higher-order effects which are induced by the presence of external gradients. These effects are due to asymmetric exit rates of particles from an individual cell when subjected to an external thermodynamical gradient and are typical of Hamiltonian dynamics. We develop a stochastic theory which explains how these asymmetries affect various aspects of heat and particle transport in systems of the general type described above. We verify our assumptions with extensive numerical simulations.

## 1 Introduction

In this paper, we study nonequilibrium transport in a class of 1-D Hamiltonian systems consisting of free noninteracting point particles of mass  $m$  (tracers) moving inside a chain of identical boxes (cells), which are like “chaotic billiards”. Each cell contains a device (called a *tank* in [1]) that interacts with the tracers by exchanging energy with them. Even though the tracers do not interact among themselves, an effective interaction is mediated by the tanks. As pointed out in

previous studies [2, 3], this mediated interaction among the tracers allows such models to reach thermalization. These models are therefore genuine many-particle interacting Hamiltonian systems [4]. Moreover, the details of the interaction between tanks and tracers are not important. However, since our aim is to study model systems with realistic microscopic dynamics we shall ask that this interaction satisfies some general conditions: The system has to be time-reversible and Hamiltonian, although conservation of phase space volume is seemingly enough.

An earlier study, [1], went some ways in explaining the energy and particle profiles in terms of a stochastic approximation to a Hamiltonian model. This class of models was derived, in turn, from work [2, 3] in which a Lorentz gas with rotating discs was considered.

The stochastic approximation used in [1] assumed that in their evolution, the tracers exit on both sides of each cell with *equal* probability, and at the same rate. Out of equilibrium, these rates will change from cell to cell and this leads to the effective transport of particles and heat. It was found that, to lowest order, due to the gradient character [5] of the system, the profiles for the rates at which particles and energy are transported among neighboring cells interpolate *linearly* between the values imposed by the baths at the ends. From this, energy and particle density along the chain were computed explicitly.

The equal probability to jump to the left or to the right leads to a simple random walk process, without any memory effects. However, for Hamiltonian deterministic systems of interacting particles the memory effects cannot in general be neglected and the symmetry assumption is likely to fail.

In this paper, we study in some detail the consequences of the violation of the symmetry assumption. For the class of 1-D Hamiltonian chains that we consider, the *reflection and transmission probabilities for particles (and energy) are not equal*. In other words, there is a (positive or negative) bias for a particle to leave the cell on the side it entered. We call this the **breaking of the RT-symmetry**. This phenomenon has a geometrical and a dynamical origin: For any scattering billiard (like the model cells) the reflection probability will in general be different from the transmission purely due to the geometry of the cell. When some source of interaction among the tracers is considered, these coefficients will depend in addition on the local thermodynamical fields (namely, density and temperature) of the tracers in the cell. When, in addition, the cell is subjected to an external thermodynamical gradient, the reflection and transmission probabilities will be different at the left and at the right of the cell. In this situation the dynamical asymmetry is emphasized.

Close to equilibrium, the geometric component dominates the dynamics, and

then the bias is *independent* of the local thermodynamical fields and thus, uniform along the chain. Furthermore, in this simpler case, the bias of the reflection/transmission coefficients is the *same* on both sides of any cell. The corresponding stochastic model is a persistent random walk process like that studied in Lorentz gases [6]. After introducing the model in Section 2, we proceed in Section 3 to a stochastic approximation. In Section 4, we study the case of constant bias and show that one recovers the gradient property observed in [1], albeit with a slight correction in the slope of the jump rate profiles.

In the final sections, we analyze how the presence of *non uniform* local fields changes this picture. Clearly, since the tanks induce an interaction of the tracers, the reflection (or transmission) probability depends on the local thermodynamical fields. We will distinguish two contributions: one that depends on the mean values of the fields and another one that depends on the local gradients of the fields. These two effects are added to the purely geometrical contribution of the corresponding non-interacting system.

In order to judge the importance of the asymmetry phenomenon, we take fixed external fields and let the number of cells be sufficiently large. This is the standard limit taken in studies of the Fourier law [7, 8]. In this setting, the system is no longer of gradient type, and we obtain expressions for the transport equations which go beyond the standard linear regime. While these equations remain approximate, we verify numerically their validity even very far from equilibrium.

## 2 The Mechanical Model

We consider a gas of noninteracting point particles of mass  $m$  that move freely inside a one-dimensional chain composed of  $N$  identical two-dimensional cells, arranged horizontally. Each cell is connected to its left and right neighbors through two openings of size  $\gamma$ .

Inside each cell there is a mechanical tank capable of storing a certain amount of energy. When a particle hits the tank, some energy exchange takes place, and this is the only interaction in the model.

While the details of this interaction are largely irrelevant for the discussion in this paper, our simulations have been done for the following precise setup which we call the rotating disc model (RDM). Each cell has the geometry described in Fig. 1. The energy tank is modeled by a freely rotating disc which is pinned at the center of the cell. Its energy is only rotational. When a particle hits the disc, it exchanges its tangential velocity  $v_t$  with the angular velocity  $\omega$  of the disc, while

the normal component  $v_n$  is reflected [2]:

$$\omega' = v_t, \quad v'_t = \omega, \quad v'_n = -v_n. \quad (2.1)$$

Note that while the particles do not see each other, they effectively interact through their collisions with the tanks. Thus local equilibrium can be reached [9]. The model is by no means free.

The chain is connected at both ends to two reservoirs of particles through openings of the same size  $\gamma$ . The reservoirs are idealized as infinite chambers containing an ideal gas at a certain density  $n$  and temperature  $T$ . To study non-equilibrium effects,  $n$  and  $T$  will differ at both ends.

Another variant of this model has the same fixed walls, but the disc is replaced by a rotating needle, with elastic collision, conserving total energy (and total angular momentum).

These models are among a class of models satisfying the following minimal assumptions:

- *Time reversibility:* The trajectory of the system in phase space across a scattering event must be time reversible. While this condition is not really necessary for our derivations, our aim is to model realistic macroscopic situations for which microscopic time-reversibility is believed to hold.
- *Conservation of phase-space volume:* This condition is not as strong as requiring the dynamics to be Hamiltonian, and seems to lead to similar results. In particular, the rotating disc model satisfies this condition but is not Hamiltonian: Its collision rule preserves phase space volume but is not a canonical transformation.

We call the models satisfying these two assumptions **mechanical**.

We end the description of the model by a more detailed account of the heat and particle baths. From the left reservoir at density  $n_>$  and temperature  $T_>$ , particles are injected into the system at a rate  $j_>$ . Observe that the mean energy of the tracers injected into the system is not  $T_>$  but  $\frac{3}{2}T_>$  (see *e.g.*, [1]). Thus, the left reservoir injects energy into the system at a rate  $q_>$  given by

$$q_> = \frac{3}{2} j_> T_>.$$

Analogously, the right reservoir injects particles and energy at rates  $j_<$  and  $q_<$  respectively. Each injected particle will be eventually re-absorbed by one of the reservoirs and this happens when it crosses into that reservoir.

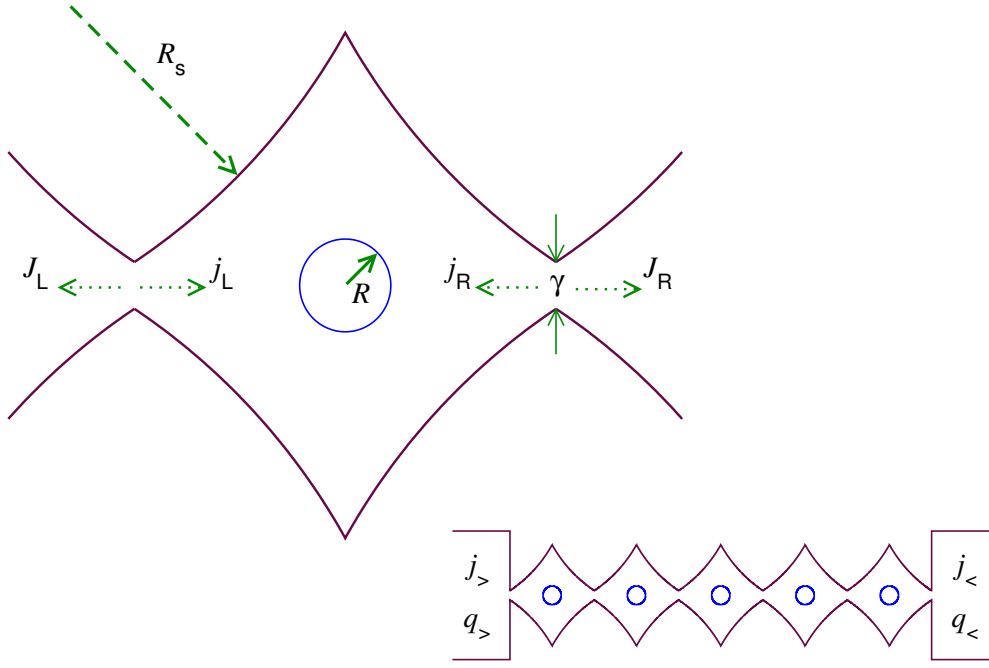


Figure 1: Upper left: The geometry of a single cell for the rotating disc model. The boundary of the cell is made of four arcs of circles of radius  $R_s$ . The radius  $R$  of the rotating disc is chosen so that no trajectory can cross the cell without undergoing any collision. The arrows represent the incoming ( $j$ ) and outgoing ( $J$ ) rates of particles that cross the exits of width  $\gamma$ . The rates  $q$  and  $Q$  for the energy are not shown. Lower right: A chain of 5 cells connected to two baths.

As the reservoirs consist of an ideal gas the injection rate  $j$  is a function of the density  $n$  and temperature of the reservoir given by

$$j \propto \gamma n T^{1/2}. \quad (2.2)$$

Furthermore, the chemical potential at the reservoirs can be written in terms of the injection rate as

$$\mu = T \log \left( \frac{\lambda_0 j}{T^{3/2}} \right) \quad (2.3)$$

with  $\lambda_0$  some constant.

We end the section with some comments on the choice of the model: Our choice of the reflecting boundaries of Fig. 1 is to guarantee the desirable ergodic and mixing properties of chaotic billiards. However, we have not succeeded in

showing rigorously that the cell is either ergodic or mixing. While the geometry of the rotating needles model (RNM) is similar to that of the RDM, there are two main differences: First, the RNM is not only mechanical but Hamiltonian. Second, in the RNM model, a particle can in principle cross many cells without hitting any needles or boundaries. This may produce logarithmic corrections to transport, which are beyond our study.

### 3 The Stochastic Model

In [1], a stochastic approximation of the mechanical model was considered. In this approximation it was assumed that what happens in one cell is independent of the state of the other cells. The particles perform a random walk among the cells, mixing their energies with the tanks according to rules which mimic the mechanical system described above. Once the particle has mixed its energy, it waits (until an exponential clock rings) and then jumps with equal probability to the left or to the right. With these assumptions it was found that the rates at which particles and energy jump among neighboring cells are linear functions of the position and from this, energy and particle density along the chain can be computed explicitly under very general assumptions.

The purpose of this paper is to study the consequences of relaxing the condition of symmetric exits. Because of the mechanical nature of the interaction, tracers will remember their history, and we want to take into account some memory effects in an improved stochastic model.

These memory effects will be described by a set of parameters which describe the reflection and transmission of both particles and the energy carried by them. It is convenient to distinguish the local *incoming* rates from the *outgoing* rates. We denote by  $J_{L,k}$  and  $Q_{L,k}$  the rates at which particles and energy exit the  $k$ -th cell to the left and by  $J_{R,k}$ ,  $Q_{R,k}$  those to the right. The exit rates are then simply determined by the corresponding incoming rates  $j_{L/R,k}$  and  $q_{L/R,k}$ , and by reflection  $\alpha_{L,k}$ ,  $\alpha_{R,k}$  coefficients which will satisfy the balance equations (for the

cell  $k$ ):

$$\begin{aligned} J_{L,k} &= \alpha_{L,k}^J j_{L,k} + (1 - \alpha_{R,k}^J) j_{R,k}, \\ J_{R,k} &= (1 - \alpha_{L,k}^J) j_{L,k} + \alpha_{R,k}^J j_{R,k}, \\ Q_{L,k} &= \alpha_{L,k}^Q q_{L,k} + (1 - \alpha_{R,k}^Q) q_{R,k}, \\ Q_{R,k} &= (1 - \alpha_{L,k}^Q) q_{L,k} + \alpha_{R,k}^Q q_{R,k}. \end{aligned} \tag{3.1}$$

Note that even for (left-right) symmetric cells, out of equilibrium the reflection coefficients at the left and right of the cell are not necessarily equal. The balance equations account for the conservation of energy and particle number, namely  $Q_{L,k} + Q_{R,k} = q_{L,k} + q_{R,k}$  and  $J_{L,k} + J_{R,k} = j_{L,k} + j_{R,k}$ .

We define the coefficients by empirical probabilities  $j_{LR} \dots$  by (omitting the index  $k$  for better legibility)

$$\begin{aligned} \alpha_L^J &= \frac{j_{LL}}{j_L}, & \alpha_R^J &= \frac{j_{RR}}{j_R}, \\ \alpha_L^Q &= \frac{1}{2} + \frac{q_{LL} - q_{LR}}{2q_L}, & \alpha_R^Q &= \frac{1}{2} + \frac{q_{RR} - q_{RL}}{2q_R}, \end{aligned} \tag{3.2}$$

where, for example,  $j_{LR}$  is the rate of particles leaving on the right, which entered on the left, and  $q_{LR}$  is the mean energy carried out by them. The definition for the  $\alpha^J$  is canonical, but for the  $\alpha^Q$  we chose a more complicated expression: It simultaneously preserves total energy conservation, but allows for an energy change during scattering.

The dynamics of the stochastic model is defined as follows: We consider a set of particles moving inside a one-dimensional chain of  $N$  cells. Inside each cell there is a scatterer with which particles make instantaneous collisions. When a particle enters the cell  $k$  the probability to move (transfer energy) forward or backwards is given by the reflection probabilities controlled by (3.1). A steady state is maintained by injecting particles and energy into the chain from the left and from the right at rates  $j_>, q_>$  and  $j_<, q_<$  respectively.

To simplify the discussion, we make the approximate assumption that the  $\alpha_Y^X$  (for all  $X \in \{J, Q\}$  and  $Y \in \{L, R\}$ ) only depend on the incoming fluxes. Due to the mechanical nature of the models considered here, the time scale is a free variable leading to the scaling relation

$$\alpha(j_L, j_R, q_L, q_R) = \alpha(\lambda j_L, \lambda j_R, \lambda^3 q_L, \lambda^3 q_R), \tag{3.3}$$

for all  $\lambda > 0$ . Therefore,  $\alpha$  only depends on 3 ratios. It will be useful to distinguish the contribution to  $\alpha$  that arises out of equilibrium from the contribution that only depends on the mean values of the fields. Accordingly we write

$$\alpha(j_L, j_R, q_L, q_R) = \alpha_G \left( \frac{j^{3/2}}{q^{1/2}} \right) + \varepsilon \left( \frac{j^{3/2}}{q^{1/2}}, \frac{j_R - j_L}{j_R + j_L}, \frac{q_R - q_L}{q_R + q_L} \right), \quad (3.4)$$

and require that  $\varepsilon(j^{3/2}/q^{1/2}, 0, 0) = 0$ , *i.e.*, that  $\varepsilon$  vanishes at equilibrium. The term  $\alpha_G$ , which has a purely geometric origin, describes in turns those aspects which hold at thermal equilibrium and the term  $j^{3/2}/q^{1/2}$ , with  $q = (q_L + q_R)/2$  and  $j = (j_L + j_R)/2$ , is proportional to the density (see Eq. (2.2)). In what follows we will refer to  $\alpha_G$  as *bias* and to  $\varepsilon$  as *asymmetry*.

The meaning of the  $\alpha_Y^X$  is illustrated for some special cases: The case  $\alpha_Y^X = \frac{1}{2}$  corresponds to the simple symmetric random walk considered in [1], *i.e.*. The case when the  $\alpha_Y^X$  are independent of the local fields, but different from  $\frac{1}{2}$  corresponds to a persistent random walk and will be studied in the next section. More realistic laws will be investigated in the last sections.

In the stochastic model the details of the dynamics, in particular those that depend on the specific model, are encoded by Eq. 3.4. To show the validity of our approach and of the stochastic model we will proceed as follow: Under general reasoning we first specify the law (3.4). This closes the balance equations for the jump rates. We next determine the thermodynamical profiles and currents. Finally we compare these “theoretical” profiles to those obtained with numerical simulations of the mechanical model.

## 4 Solution of the Stochastic Model Near Equilibrium

In this section, we discuss profiles in the infinite volume limit with fixed boundary conditions, under the approximating assumption that every cell is at local equilibrium. This means to neglect the term  $\varepsilon$  in Eq. (3.4) and thus,  $\alpha_{R,k}^J = \alpha_{L,k}^J = \alpha_G^J$  and similarly for the  $\alpha^Q$ . Furthermore, we make the assumption, that  $\alpha_G^J$  and  $\alpha_G^Q$  are independent of the densities found in the chain. In this approximation the reflection coefficient is a constant independent of the thermodynamical fields and thus, independent of position. The exact range of validity of this assumption will be discussed in Sec. 5.

Since the geometric contribution is the only one remaining in (3.4), we refer to this case as the **geometric approximation**. Note that this contribution will leads in general to a reflection coefficient different from  $\frac{1}{2}$ . This approximation

corresponds to a persistent random walk in which the probability for the walker to move forwards is different from the probability to move backwards.

We discuss the total ejection rates  $J_k = J_{L,k} + J_{R,k}$  and  $Q_k = Q_{L,k} + Q_{R,k}$ . The boundary conditions of the problem are simply

$$j_> = j_{L,1}, \quad j_< = j_{R,N}, \quad q_> = q_{L,1}, \quad q_< = q_{R,N}. \quad (4.1)$$

From now on we will use rescaled variables  $\xi = k/(N+1) \in [0, 1]$ , and let  $J(\xi) = J_k$  and  $Q(\xi) = Q_k$ . For the sake of simplicity, we will only write  $\alpha^J$  and  $\alpha^Q$ .

**Lemma 4.1** *Under the assumptions made above, the particle and energy ejection rates satisfy*

$$J(\xi) = 2(j_> + \xi \cdot \Delta j) + \frac{(1 - 2\alpha^J)(1 - 2\xi)}{1 + (N-1)\alpha^J} \Delta j, \quad (4.2)$$

where  $\Delta j = j_< - j_>$ , and

$$Q(\xi) = 2(q_> + \xi \cdot \Delta q) + \frac{(1 - 2\alpha^Q)(1 - 2\xi)}{1 + (N-1)\alpha^Q} \Delta q, \quad (4.3)$$

with  $\Delta q = q_< - q_>$ .

**Remarks:** The first term in the *r.h.s.* of Eqs. (4.2) and (4.3) corresponds to the result obtained in [1]. The last terms account for the correction when  $\alpha \neq \frac{1}{2}$ . These corrections disappear in the infinite volume limit. The integral over  $\xi$  of the correction vanishes, because of energy and particle conservation. Also, note that as  $\alpha$  is a constant, the profiles are linear (even when  $\alpha \neq \frac{1}{2}$ ), because the system is still of gradient type.

**Proof:** The proof is just a calculation. We will concentrate on the case of particle rates. This calculation starts from (3.1). Using the identities Eq.(4.1), we can solve (3.1) for the remaining  $J$  and obtain for  $k = 1, \dots, N$ ,

$$\begin{aligned} J_{L,k} &= \frac{(N-k+1)\alpha}{1+(N-1)\alpha} j_> + \frac{1+(k-2)\alpha}{1+(N-1)\alpha} j_<, \\ J_{R,k} &= \frac{1+(N-k-1)\alpha}{1+(N-1)\alpha} j_> + \frac{k\alpha}{1+(N-1)\alpha} j_<. \end{aligned} \quad (4.4)$$

Then, summing the R and L terms, we get

$$J_k = \frac{1+2(N-k)\alpha}{1+(N-1)\alpha} j_> + \frac{1+2(k-1)\alpha}{1+(N-1)\alpha} j_<. \quad (4.5)$$

Rearranging terms one immediately obtains (4.2). The case (4.3) is handled similarly.

Therefore, if the value for  $\alpha$  is known, the profile of the ejection rates can be obtained from the solution (4.4) for any nonequilibrium state, as long as  $\alpha$  is independent of the external parameters.

#### 4.1 Thermodynamical profiles

Applying now the equations of [1], the profiles (4.2) and (4.3) lead, under the assumption of local equilibrium, to predictions for the mean energy  $T(\xi)$  of the tank and the mean number of particles  $n(\xi)$  at any site  $\xi = k/(N + 1)$ :

$$T(\xi) = \frac{2}{3} \frac{Q(\xi)}{J(\xi)}; \quad (4.6)$$

$$n(\xi) = \eta_0 \frac{J^{3/2}(\xi)}{Q^{1/2}(\xi)}; \quad (4.7)$$

the constant  $\eta_0$  depends only on the geometry of the cell. For that described in Fig. 1, one has

$$\eta_0 = \sqrt{\frac{3\pi}{4}} \frac{\text{Area}(\Gamma)}{|\gamma|}, \quad (4.8)$$

where the area is that of the cell minus the disc and where  $|\gamma|$  is the size of the opening between adjacent cells. These formulas become more precise when the opening is small. This choice guarantees better mixing but, when pushed too far, slows down the convergence of numerical simulations to stationarity.

To test these results we performed out of (but close to) equilibrium simulations for a chain of 20 RDM cells with  $|\gamma| = 0.04$ ,  $R_s = 1.15$  and a disc radius of  $R = 0.0793$  (ensuring that no tracer can cross a cell without being scattered). The baths were set to  $j_> = 10$ ,  $j_< = 12$ ,  $T_> = 1000$  and  $T_< = 1100$ .

We checked in our simulations that the profiles of the outgoing rates are described by (4.2) and (4.3). We first numerically computed the reflection coefficients  $\alpha^J$  and  $\alpha^Q$  for each cell. For the imposed gradient we found that both coefficients are constant (to within numerical accuracy) along the chain. From this we extracted a mean value of  $\alpha^J = 0.552 \pm 0.007$  and  $\alpha^Q = 0.553 \pm 0.006$ . We insert these values into (4.2)–(4.3) and obtain estimates for the profiles  $J(\xi)$  and  $Q(\xi)$ . We then use these estimates in (4.6) and (4.7) to obtain the profiles for the energy  $T$  and the number of particles  $n$ , as predicted by the theory based in the breaking of the RT-symmetry. These are shown as dashed lines in Fig. 2. The

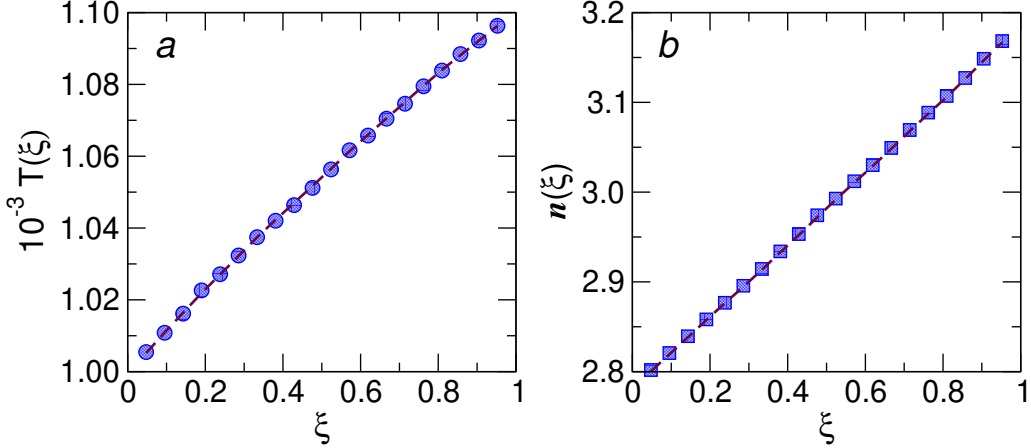


Figure 2: Profiles obtained as an average over 200 different realizations of the RDM (see the text for the details of the simulation). We show in symbols: *a*) the energy profile  $T(\xi)$  and *b*) the particle density profile  $n(\xi)$  as a function of the rescaled position. The dashed lines in each panel correspond to the theoretical profiles of Eqs. (4.6) and (4.7).

fit with the directly measured profiles for  $T$  and  $n$  is excellent. Note that these profiles are not expected to be linear [1].

#### 4.2 Macroscopic currents

The heat and matter local macroscopic currents can be easily derived from the balance equations. The current of particles between the  $k$ -th and  $k + 1$ -st cells is defined as  $\varphi^J = J_{R,k} - j_{R,k}$  or, in terms of outgoing jump rates as  $\varphi^J = J_{R,k} - J_{L,k+1}$ . Using Eq. (4.4) we obtain

$$\varphi^J = -\frac{1 - \alpha^J}{1 + (N - 1)\alpha^J} \Delta j , \quad (4.9)$$

where the result is of course independent of  $k$ . In an analogous way,  $\varphi^Q = Q_{R,k} - Q_{L,k+1}$ , and we obtain for the heat current

$$\varphi^Q = -\frac{1 - \alpha^Q}{1 + (N - 1)\alpha^Q} \Delta q . \quad (4.10)$$

Moreover, both currents are linear functions of the external gradients, thus satisfying the linear phenomenological transport equations.

In the numerical simulation described above, we also computed the heat and matter currents obtaining an average value of  $\varphi^J = -0.0781 \pm 0.0009$  and  $\varphi^Q = -186.8 \pm 0.05$ . If instead we insert the numerically computed values for  $\alpha^J$  and  $\alpha^Q$  into Eqs. (4.9) and (4.10) we obtain  $\varphi^J = -0.078$  and  $\varphi^Q = -186.5$  in perfect agreement with the numerical experiment.

Therefore, in cases in which the  $\alpha$  probability can be taken to be constant along the chain, the conclusions of Lemma 4.1 describe remarkably well the transport properties of the disc model. Similar results were found for the needle model, and we conjecture that this extends to many similar models.

To discuss the physics of macroscopic transport we assume that the gas of particles in each cell can be modeled as an ideal gas at local equilibrium. One can then express the currents in terms of the thermodynamical forces, (temperature and chemical potential) [10]. Using Eqs. (2.2) and (2.3) we can express the gradient of the injection rate  $\nabla j = \Delta j/N$  in terms of  $\nabla(1/T)$  and  $\nabla(-\mu/T)$ :

$$\varphi^J = \frac{3R(N, \alpha^J)}{4\eta_0} n T^{3/2} \nabla \left( \frac{1}{T} \right) + \frac{R(N, \alpha^J)}{2\eta_0} n T^{1/2} \nabla \left( -\frac{\mu}{T} \right), \quad (4.11)$$

and analogously for the energy current

$$\varphi^Q = \frac{15R(N, \alpha^Q)}{8\eta_0} n T^{5/2} \nabla \left( \frac{1}{T} \right) + \frac{3R(N, \alpha^Q)}{4\eta_0} n T^{3/2} \nabla \left( -\frac{\mu}{T} \right), \quad (4.12)$$

with

$$R(N, \alpha) = \frac{N(1 - \alpha)}{1 + (N - 1)\alpha}, \quad (4.13)$$

and  $\eta_0$  as in (4.8). We expect [11] the Onsager relations to hold in our model (near equilibrium). However, because  $\alpha^J \neq \alpha^Q$ , the equations above violate them. We attribute this discrepancy to the various approximations we have made in reaching (4.11) and (4.12). The origin of the inequality  $\alpha^J \neq \alpha^Q$  will be discussed in Sect. 5.

From Eq. (4.11) we can derive an expression for the diffusion coefficient. Using again Eqs. (2.2) and (2.3) we can write Eq. (4.11) in terms of the particle density gradient. When a temperature gradient is negligible we obtain Fick's law

$$\varphi^J = -\frac{R(N, \alpha^J)}{2\eta_0} T^{1/2} \nabla n, \quad (4.14)$$

from which the diffusion coefficient is easily identified. Note that the functional dependence of the diffusion coefficient on  $\alpha$  (4.13) coincides with the diffusion

coefficient for a persistent random walk process [6]. In an analogous way our model satisfies Fourier's law

$$\varphi^Q = -\frac{9R(N, \alpha^Q)}{8\eta_0} n T^{1/2} \nabla T. \quad (4.15)$$

The validity of the linear transport equations (4.14) and (4.15) is based on the property that  $\alpha_L = \alpha_R$ . For high gradients, this property will be violated as we show in Sec. 6. In that case, the Fourier law does not hold, but the flux still scales as  $1/N$  for large systems. The reason is that local gradients appear in the diffusion constants.

We remark finally that  $\alpha$  (and thus the details of the cell) determines the nature of the macroscopic transport: If  $\alpha = 0$  the transport along the chain is ballistic as the currents do not scale with the size of the system  $N$ . On the other hand, if  $\alpha = 1$  the chain behaves as an insulator. For any other value of  $\alpha$  the transport is normal with well defined transport coefficients.

## 5 Validity of the Geometric Approximation

In the previous section, we assumed that the reflection coefficient  $\alpha$ , while not necessarily equal to  $\frac{1}{2}$ , neither depends on the particle density inside a cell nor on the strain acting on it. In other words,  $\alpha_{R,k}^J = \alpha_{L,k}^J = \alpha_G^J$ , this value being determined by the geometry of the cell only (and similarly for  $\alpha^Q$ ).

In this section we discuss this assumption and determine the range of parameters for which it applies with high precision. The discussion will also clarify the choice of the decomposition (3.4). The profiles obtained when  $\alpha_R$  and  $\alpha_L$  are different and vary along the chain are discussed in the next section.

The reader should first note a simple fact: When the discs (tanks) in the cells are not allowed to rotate, and the reflection is specular, then the trajectories are independent of the energy and of the particle density. In that case  $\alpha$  is clearly independent of all external parameters (and  $\alpha^J = \alpha^Q$  since the tracers are the only energy carriers). Therefore, any variation of  $\alpha$  has its origin in the effective interaction of the tracers.

The interaction changes the dynamics inside the cell, but does not always induce a variation of  $\alpha$ . We first consider an ideal case: tracers are always trapped in the cell for a very long time. They collide with the tank many times, and forget the side from which they entered the cell, as well as the energy they had at that time. In this case, the thermalization of the tracers is perfect *due to the interaction* and neither a bias nor an asymmetry appear.

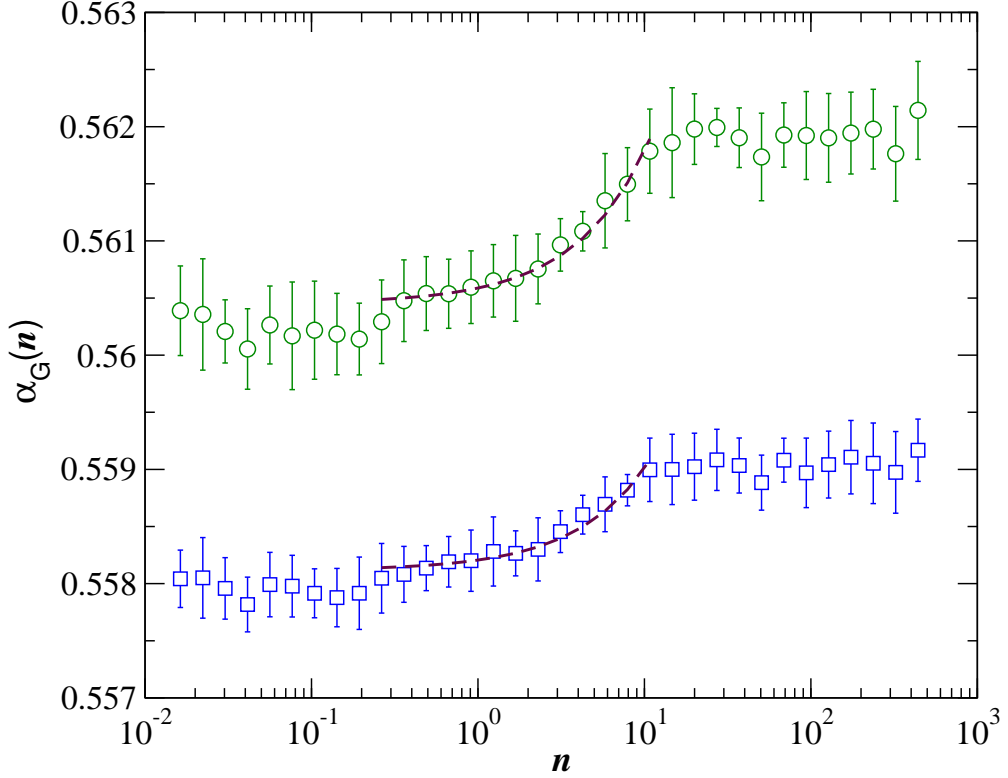


Figure 3: Dependence of the equilibrium reflection probabilities  $\alpha_G^J$  (squares) and  $\alpha_G^Q$  (circles) on the density of tracers in the cell  $n$  for the RDM with  $\gamma = 0.08$ . Note that  $\alpha_G$  saturates to a constant value at low and high densities. At intermediate densities  $0.3 < n < 10$ ,  $\alpha_G$  grows linearly with density as corroborated by the linear fits (dashed lines). The fits are  $\alpha_G^Q(n) = 0.56048 \pm 2 \cdot 10^{-5} + (1.29 \cdot 10^{-4} \pm 5 \cdot 10^{-6})n$ , and  $\alpha_G^J(n) = 0.55813 \pm 2 \cdot 10^{-5} + (8.71 \cdot 10^{-5} \pm 5 \cdot 10^{-6})n$ .

The geometric approximation loses its validity due to two related memory effects:

- The distribution of energy in the cell is not uniform, and thus thermalization is only approximate
- Particles retain a memory of the energy they had when entering the cell, and this effect is energy-dependent.

In order to test these properties, we first performed *equilibrium* simulations. In Fig. 3 we show the dependence of the reflection probabilities  $\alpha_G^J$  and  $\alpha_G^Q$  on the

density of tracers  $n$  for a single cell (for the RDM). Injection rates of the reservoirs are chosen according to (2.2) in order to obtain the desired densities. We observe the following:

- For low densities ( $n \lesssim 0.3$ ) and high densities ( $n \gtrsim 10$ ), the bias is practically constant. Therefore, if a whole chain of cells is in either of these regimes, we can model it with a constant bias. If in addition, the local gradients are small, then the system is (close to) gradient type, and is well described by the approximations of Sec. 4.
- For intermediate densities, the bias increases linearly with the density. This is a new kind of regime (not of gradient type), which we discuss in more detail in the next section.

As discussed in Sec. 3, the distinction between the bias  $\alpha_G$  and the asymmetry  $\varepsilon$  in Eq. (3.4) is that while  $\varepsilon$  depends on the local gradients of the thermodynamical field (and is zero at equilibrium),  $\alpha_G$  will depend at most on the mean fields. Therefore, we can expect that a constant reflection coefficient will always remain a good approximation close to equilibrium, namely when  $\Delta T/T \ll 1$  and  $\Delta n/n \ll 1$ . In that case, the equations of the Sec. 4 hold, regardless of the average density of the system.

The reader should observe that  $\alpha_G^Q$  and  $\alpha_G^J$  differ, while for a system without memory effect (such as the Lorentz model) one would expect equality of these quantities. This difference is not an artifact of our simulations but a property of mechanical models of the type we consider. Looking at Fig. 1, and the collision rule (2.1), the reader will realize that fast particles have a higher probability to exit after only 1 collision with the disc than slower ones, because the angle of reflection tends to be smaller for the fast ones. Therefore the memory effect depends on the individual energies and not the mean, and this accounts for the difference above. We have checked that by placing non-rotating discs between the openings and the turning disc, the effect is reduced.

We now turn our attention to *nonequilibrium* effects, which are described by the functions  $\varepsilon_Y^X$  of Eq. (3.4). We performed simulations for the single cell RDM in which the external gradients were kept fixed but the mean temperature was changed ( $T_> = T - \Delta T/2$  and  $T_< = T + \Delta T/2$ ). In the inset of Fig. 4, we show the left and right reflection coefficients,  $\alpha_L^J$  and  $\alpha_R^J$ , as a function of  $\Delta T/T$ . As the parameters approach equilibrium values, the difference  $|\alpha_L^J - \alpha_R^J|$  is seen to decay to zero (at a rate  $(\Delta T/T)^{5/2}$ ). The value that  $\alpha_L^J$  and  $\alpha_R^J$  take in equilibrium is the constant geometric asymmetry (which for these parameters are  $\alpha_G^J \sim 0.558$

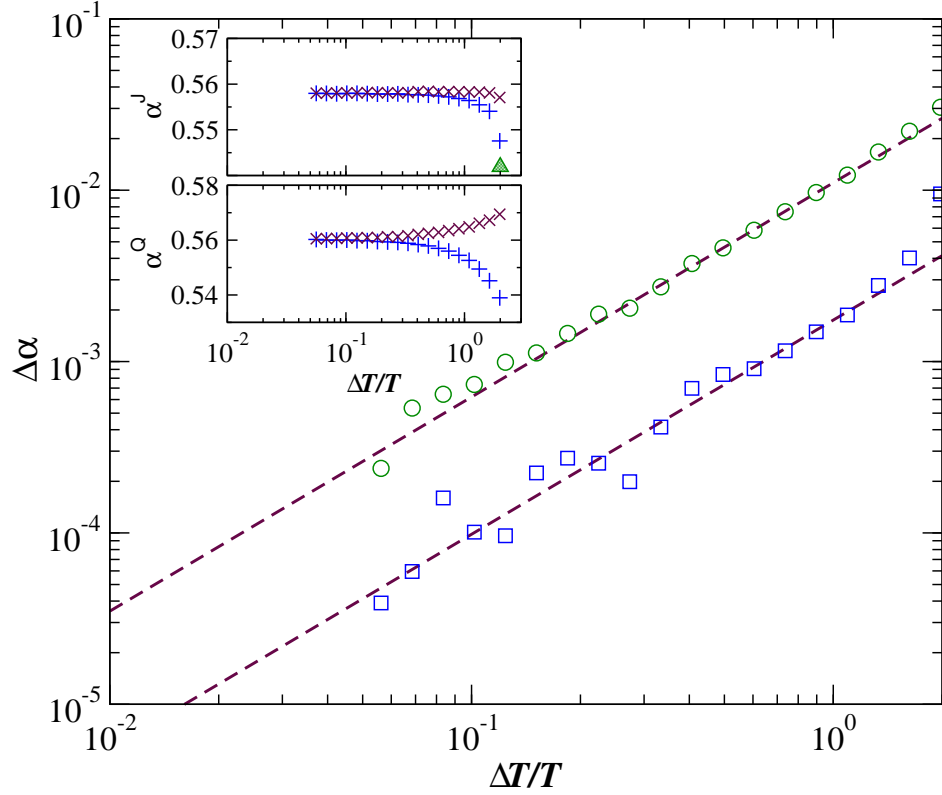


Figure 4: Difference  $\Delta\alpha = \alpha_R - \alpha_L$  as a function of  $\Delta T/T$  for  $\alpha^J$  (squares) and  $\alpha^Q$  (circles). Each symbol corresponds to a simulation for the single cell RDM with a geometry as in Fig. 2 but  $|\gamma| = 0.08$ . In all experiments the external gradients were fixed to  $j_> = j_< = 1$ ,  $\Delta T = T_< - T_> = 100$  and  $\frac{1}{2}(T_> + T_<) = T$ . The dashed lines correspond to  $\Delta\alpha \sim (\Delta T/T)^{5/2}$ . In the inset  $\alpha^J$  and  $\alpha^Q$  at the left (plus) and right (crosses) boundaries are shown. Note that  $\Delta\alpha \rightarrow 0$  on approach to equilibrium, while for very large gradients  $\alpha_L^J$  reaches the Lorentz gas limit indicated by the hashed triangle (see the text for a discussion).

and  $\alpha_G^Q \sim 0.560$ ). At the other extreme, since the temperature cannot be negative,  $\Delta T/T \leq 2$ . The difference  $\Delta\alpha$  is maximal at  $\Delta T/T = 2$ . Interestingly,  $\alpha_L^J(\Delta T/T = 2)$  corresponds to the reflection coefficient of the Lorentz gas, *i.e.*, to the limit in which the central disc does not rotate.

## 6 Far from Equilibrium

In Section 4 we have assumed that the system is at local equilibrium, and that the particle density varies in a range where the  $\alpha_G$  are essentially constant. In this section, we discuss the case when both these assumptions are dropped. This means that we take into account the dependence of the  $\alpha$  on the density and on the local gradients of the thermodynamical fields.

Far from equilibrium, the distribution of the local fields will be different from cell to cell and thus, the probabilities will depend on the position along the chain  $\alpha \equiv \alpha(\xi)$ . We recall the set of equations Eq. (3.4) for  $\alpha$  one of the functions  $\alpha_Y^X$ :

$$\alpha(j_L, j_R, q_L, q_R) = \alpha_G \left( \frac{j^{3/2}}{q^{1/2}} \right) + \varepsilon \left( \frac{j^{3/2}}{q^{1/2}}, \frac{j_R - j_L}{j_R + j_L}, \frac{q_R - q_L}{q_R + q_L} \right) .$$

It is understood that  $\alpha_G$  and  $\varepsilon$  denote functions which are different for the various  $\alpha_Y^X$ , but have the following common properties: By definition,  $\varepsilon$  must vanish at equilibrium

$$\varepsilon_Y^X(x, 0, 0) = 0 .$$

Furthermore, the left-right symmetry of the cell implies:

$$\varepsilon_L^X(x, y, z) = \varepsilon_R^X(x, -y, -z) . \quad (6.1)$$

We next discuss specific properties of  $\varepsilon$  as they appear from numerical simulations for the RDM. It turns out that the  $\varepsilon_Y^X$  not only vanish on the submanifold  $(x, 0, 0)$ , but, to a very good approximation they vanish for those points where the temperatures  $T_L$  and  $T_R$  are equal. Since the temperatures are functions of the injection rates of particles and energy this means that  $\varepsilon_Y^X$  vanishes on the submanifold of  $\{j_L, j_R, q_L, q_R\}$  where  $T_L = T_R$ . While we have no proof of this observation, it can be understood by observing that for  $T_L = T_R$  the tank has the same temperature as all the tracers, and therefore we are in presence of purely geometric phenomena which are already captured by the function  $\alpha_G$  alone.

We expand  $\varepsilon_Y^X$  to first order, and in view of the above information, a very good approximation is given by assuming that  $\varepsilon$  has the form:

$$\varepsilon = \varepsilon_0 \frac{T_R - T_L}{T_R + T_L} + \varepsilon_1 \frac{T_R - T_L}{T_R + T_L} \cdot \frac{j_R - j_L}{j_R + j_L} , \quad (6.2)$$

where  $\varepsilon_0$  and  $\varepsilon_1$  are constants depending on the choice  $X, Y$ . We have numerically corroborated Eq. (6.2) for the RDM. In Fig. 5 a contour density plot for  $\alpha_L^J$  is

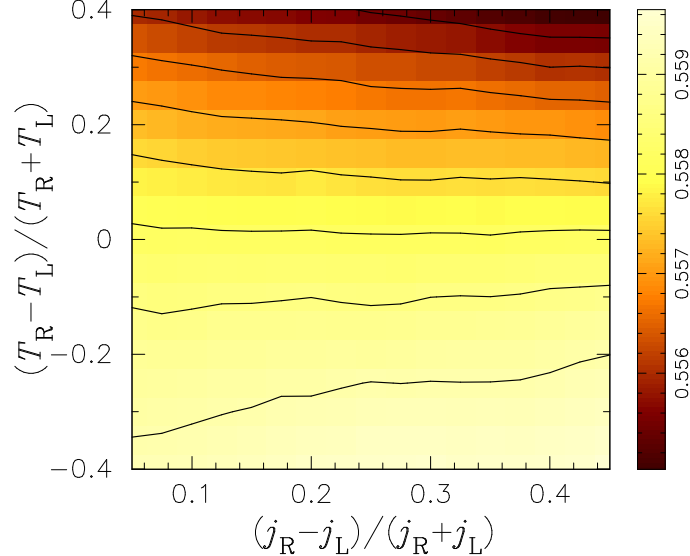


Figure 5: Contour density plot of  $\alpha_L^J$  as a function of the local gradients in  $j$  and  $T$ . The obtained values correspond to the one-cell RDM with an opening of  $\gamma = 0.08$ . Note that the contour line for  $T_L = T_R$  is horizontal, justifying Eq. (6.2).

shown as a function of the local gradients. The linearity of the contours shows that  $\alpha_L^J$  is a linear function of the local gradient in  $j$  whose slope and intercept depends on the local gradient of temperature. The same behavior is found for the other coefficients.

The reader should note that for fixed external parameters (for the heat and particle reservoirs) and for long chains, the local gradients per cell scale like  $1/N$  and thus, one expects the  $\varepsilon$  to be both proportional to  $1/N$  and to the force fields. The question then is whether the effect of the asymmetry will disappear in the infinite volume limit or not.

We next show how, in principle, the above approximations lead to a closed system of equations for the profiles, and we then check, for one particular case that the equations indeed describe the profiles found in numerical experiments, and account correctly for the deviation from [1].

Since the local gradients are naturally expressed in terms of the injection rates

we use the identification between injection and ejection rates to write Eq. (3.1) as

$$\begin{aligned} j_{R,k-1} &= \alpha_{L,k}^J j_{L,k} + (1 - \alpha_{R,k}^J) j_{R,k} , \\ j_{L,k+1} &= (1 - \alpha_{L,k}^J) j_{L,k} + \alpha_{R,k}^J j_{R,k} , \end{aligned} \quad (6.3)$$

with  $k = 1, \dots, N$  and boundary conditions  $j_{L,1} = j_>$  and  $j_{R,N} = j_<$ .

Using the definition of the particle current  $\varphi^J = j_{L,k+1} - j_{R,k}$ , one can eliminate the  $j_R$  (or the  $j_L$ ), and the Eqs. (6.3) in which case the system reduces to only one equation:

$$(1 - \alpha_{L,k}^J) j_{L,k} - (1 - \alpha_{R,k}^J) j_{L,k+1} + \alpha_{R,k}^J \varphi^J = 0 . \quad (6.4)$$

Analogous expressions are obtained for the energy injection rates.

It is here that the non-gradient nature of our models is visible in a nutshell. For (6.4) to be of gradient type one needs to have  $\alpha_{L,k}^J = \alpha_{R,k}^J$ . As we have seen in Fig. 4, this is, in general, not the case.

## 6.1 Infinite volume limit

We take the continuum limit of Eq. (6.4), with cells of size  $1/N$  so that the rescaled variable  $\xi = k/(N+1)$  is in the domain  $[0, 1]$ . Note that the currents  $\varphi^J$  and  $\varphi^Q$  scale (for fixed external forces) like  $1/N$ .

In order to close the balance equation for  $j_L$  one substitutes the ansatz (6.2) into Eq. (6.4). This leads to an involved, but in principle straightforward system of nonlinear differential equations, which we do not write down. However, we will deal with the special simpler case in which  $q(\xi)$  is approximately constant along the chain.

When  $q$  is constant, one finds that  $T \propto 1/j$  and therefore the assumption (6.2) can be reformulated for the corresponding  $\varepsilon_L$  and  $\varepsilon_R$  to first order in  $1/N$  as

$$\varepsilon_{L,k}^J = \mathcal{A}^J \frac{j_{R,k} - j_{L,k}}{j_{R,k} + j_{L,k}} , \quad \varepsilon_{R,k}^J = -\mathcal{A}^J \frac{j_{R,k} - j_{L,k}}{j_{R,k} + j_{L,k}} , \quad (6.5)$$

where  $\mathcal{A}^J = -\varepsilon_0$  are constants determined by the boundary conditions of (6.4). The minus sign in the equation for  $\varepsilon_{R,k}^J$  is a direct consequence of (6.1).

We have numerically corroborated the hypothesis (6.5). In Fig. 6 we show the dependence of the asymmetries  $\varepsilon^J$  and  $\varepsilon^Q$  on the gradients of the local injection rates for a chain of 20 RDM cells. The asymmetries are seen to depend linearly on the local gradient of  $j$ . Farther from equilibrium (not shown), deviations will appear.

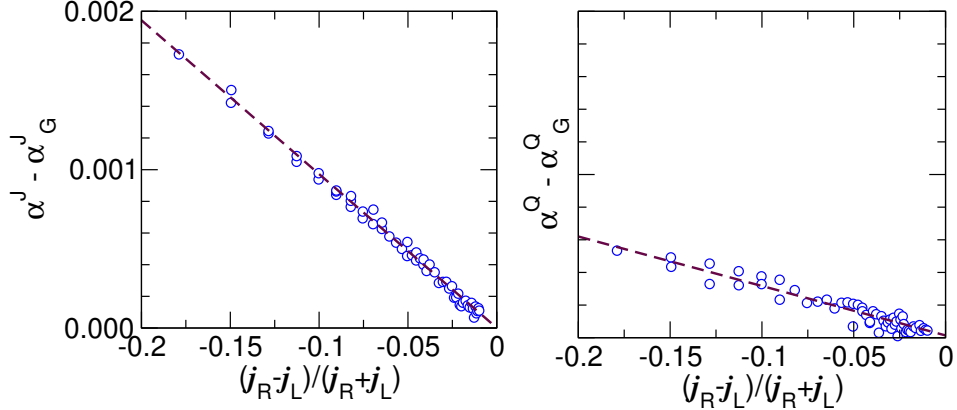


Figure 6: Dependence of the left (squares) and right (circles) reflection probabilities  $\alpha^J - \alpha_G^Q$  and  $\alpha_G^Q$  on the gradients of the local fields for a chain of 20 RDM cells with  $\gamma = 0.08$ . The external gradients were fixed to  $j_> = 1$ ,  $j_< = 6$ , and  $q_> = q_< = 1500$ . The values for the  $\alpha_G$  have been taken from the data of Fig. 3.

Using the particle current we express the asymmetry (6.5) in terms of the  $j_L$  alone as

$$\begin{aligned} \varepsilon_{L,k}^J &= \mathcal{A}^J \frac{j_{L,k+1} - j_{L,k} - \varphi^J}{j_{L,k+1} + j_{L,k} - \varphi^J}, \\ \varepsilon_{R,k}^J &= -\mathcal{A}^J \frac{j_{L,k+1} - j_{L,k} - \varphi^J}{j_{L,k+1} + j_{L,k} - \varphi^J}. \end{aligned} \quad (6.6)$$

Finally, inserting (6.6) into (6.4) we obtain a closed equation for  $j_L$  with only one system dependent free parameter,  $\mathcal{A}^J$ . In the scaling limit one finds the following nonlinear differential equation for the injection rates:

$$j_L'(\xi) = -\frac{\alpha_G^J(n(\xi)) - \mathcal{A}^J}{1 - \alpha_G^J(n(\xi)) + \mathcal{A}^J} (N\varphi^J) + \mathcal{O}\left(\frac{1}{N}\right). \quad (6.7)$$

The same equations hold for the “R” versions but with different boundary conditions.

Note that  $\varphi^J$  is the current of a chain of length  $N$ , and hence is asymptotically equal to  $\Phi^J/N$ . Using (6.7),  $\Phi^J$  can be determined by the boundary conditions as

$$\Phi^J = \frac{j_> - j_<}{\int_0^1 W^J(\xi) d\xi},$$

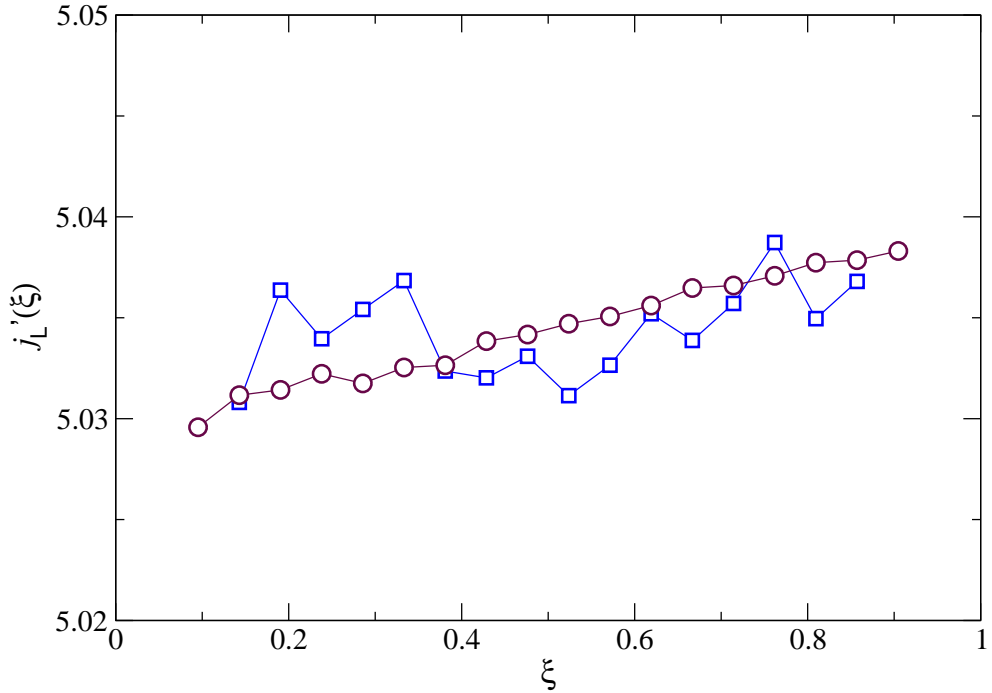


Figure 7: Numerical verification of Eq. (6.7), for  $j'_L$ , for systems of size  $N = 20$ . The external parameters are those of Fig. 6. The circles correspond to the r.h.s. of (6.7) as explained in the text, while the squares correspond to  $(j_{L,k+1} - j_{L,k})(N + 1)$ —measured at  $\xi = k/(N + 1)$ —which is an approximation to  $j'_L(\xi)$ .

where  $W^J(\xi)$  is the coefficient of  $\varphi^J$  in Eq. (6.7).

As discussed in Sec. 5 (see *e.g.*, Fig. 3), we have found that at sufficiently low or high densities, the bias depends little on the local fields, taking practically a constant value. Therefore, if the external gradient imposed by the injection of the reservoirs into the system is such that the density in all the cells of the chain is either low ( $n \lesssim 0.3$ ) or high ( $n \gtrsim 10$ ) then the bias  $\alpha_G(n(\xi))$  can be taken as constant along the chain. In this situation Eq. (6.7) gives a linear profile for the injection rate,  $\partial_\xi j_L(\xi) = \text{const}$ . In particular, in the high density regime, linear profiles will be obtained even when the gradients are very large and the system is far from equilibrium.

For intermediate densities, it follows from (3.4) that  $\alpha_G$  is a function of

$$\sqrt{\frac{(j_L + j_R)^3}{q_L + q_R}},$$

which to lowest order in  $1/N$  is

$$n(\xi) \propto \sqrt{\frac{j_L^3(\xi)}{q_L(\xi)}}. \quad (6.8)$$

Therefore, in the intermediate density regime, where we have found that  $\alpha_G(n)$  is a linear function of  $n$ , Eq. (6.7) leads to a system of two explicit coupled differential equations for  $j$  and  $q$ , which can be solved.

The consistency of our approximations was checked for the RDM model by combining the measurements of all the quantities appearing in Eq. (6.7). The results for the discrete version of this equation are summarized in Fig. 7, which shows good agreement with the theory. The external parameters used are those of Fig. 6, which guarantee that all densities along the chain lie in the domain of linear dependence shown in Fig. 3, *i.e.*, between 0.3 and 10. The data in Fig. 7 were obtained as follows: The derivatives  $j'_L$  were approximated with centered differences along the profiles. The bias  $\alpha_G$  was read off the linear fit of Fig. 3. The flux  $\varphi$  is directly read off the simulations, while the  $\mathcal{A}$  coefficients are obtained from the slope in Fig. 6.

## 7 Conclusions

In this paper we have developed a stochastic approximation for the dynamics of a family of Hamiltonian models of many interacting particles. This stochastic model is based on a detailed analysis of the way in which particles and energy are transported along the system. It captures the essential features of the microscopic dynamics including memory effects inherent to any Hamiltonian deterministic dynamics.

Close to equilibrium the correction due to these memory effects preserves the gradient character of the system. The stochastic approximation predicts with high precision the transport properties of our class of Hamiltonian models, namely the fluxes of heat and matter and the steady state energy and density profiles.

Far from equilibrium, the memory effects strongly depend on the local gradients of the thermodynamical fields and thus, on the particular interaction between

particles and energy tanks. We have shown that in the continuum limit the system is no longer of gradient type and the energy and particle currents are not proportional to the external gradients. However, the gradient type condition is restored in the limit of very high or very low densities.

Given that the dynamical memory effects depend on the particular nature of the interaction, our explicit solution (*e.g.*, the particular case of (6.7)), cannot be applied to a general context. However, the program outlined and the variables used in our derivation are valid and appropriate for the family of models that we have considered.

### Acknowledgments

This work was partially supported by the Fonds National Suisse.

## References

- [1] J.-P. Eckmann and L.-S. Young. Nonequilibrium energy profiles for a class of 1-d models. *ArXiv:nlin.CD/0504005*
- [2] C. Mej  a-Monasterio, H. Larralde, and F. Leyvraz. Coupled normal heat and matter transport in a simple model system. *Phys. Rev. Lett.* **86** (2001), 5417–5420.
- [3] H. Larralde, F. Leyvraz, and C. Mej  a-Monasterio. Transport properties of a modified Lorentz gas. *J. Stat. Phys.* **113** (2003), 197–231.
- [4] E.G.D. Cohen and L. Rondoni. On some derivations of irreversible thermodynamics from dynamical systems theory. *Physica D* **168** (2002), 341–355.
- [5] H. Spohn. *Large Scale Dynamics of Interacting Particles*. Text and monographs in Physics (Heidelberg: Springer-Verlag, 1991)
- [6] H. van Beijeren. Transport properties of stochastic Lorentz models. *Rev. Mod. Phys.* **54** (1982), 195–234.
- [7] F. Bonetto, J.L. Lebowitz, and L. Rey-Bellet. Fourier’s law: a challenge for theorists. In: *Mathematical Physics 2000* (London: Imp. Coll. Press, 2000) pp. 128–150.
- [8] S. Lepri, R. Livi, and A. Politi. Thermal conduction in classical low-dimensional lattices. *Phys. Rep.* **377** (2003), 1–80.
- [9] A. Dhar and D. Dhar. Absence of local thermal equilibrium in two simple models of heat conduction. *Phys. Rev. Lett.* **82** (1998), 480.
- [10] S. R. de Groot and P. Mazur. *Non-equilibrium Thermodynamics* (Dover, New York, 1984).

[11] G. Gallavotti and D. Ruelle. SRB states and nonequilibrium statistical mechanics close to equilibrium *Commun. Math. Physics* **190** (1997), 279–285.